

High-Speed 850 nm Photodetector for Zero-Bias Operation

Zhiyang Xie , Zhiqi Zhou, Linze Li, Zhuo Deng , Haiming Ji, and Baile Chen 

Abstract—High-speed photodetector operating at 850 nm wavelength with a large diameter and high quantum efficiency is desirable to meet the growing demands of short-reach optical links for high-performance computing systems. Zero-bias operation of the high-speed photodetectors can reduce power consumption, minimize system complexity of the optical transceivers and reduce the radiation damage in a harsh environment. Traditional p-i-n photodetectors for 850 nm applications often require a high reverse bias to accelerate the carrier transport for high-speed data transmission. In this work, we demonstrate a high-speed and low dark current modified uni-traveling-carrier photodiode based on GaAs/AlGaAs at 850 nm wavelength operating under zero bias with a quantum efficiency of 73%. The 3-dB bandwidth of the 20 μm and 40 μm diameter devices is 22.5 GHz and 13.3 GHz, respectively. A clear eye pattern is demonstrated at a 25.8 Gbit/s data rate for the device under zero-bias operation. To the best of our knowledge, this photodetector demonstrates the highest 3-dB bandwidth among all the zero-bias 850 nm photodetectors reported to date.

Index Terms—850 nm wavelength photodetector, high-speed photodetector, low dark current, zero-bias operation.

I. INTRODUCTION

SHORT distance optical links based on high-speed optical transceivers and multimode fibers (MMFs) have many applications in high-performance computing (HPC) systems [1], [2]. The multimode 850 nm GaAs VCSELs, with the advantage of low cost, low threshold current, and high modulation bandwidth, have been demonstrated [3]. Meanwhile, high-speed, high quantum efficiency, low dark current photodetectors operating at 850 nm are demanded in order to handle the exponential growth of the volume of data traffic.

Manuscript received April 14, 2021; revised July 3, 2021; accepted July 5, 2021. Date of publication July 7, 2021; date of current version August 9, 2021. This work was supported by the National Key Research and Development Program of China under Grant 2018YFB2201000. (Corresponding author: Baile Chen.)

Zhiyang Xie is with the School of Information Science and Technology, ShanghaiTech University, Shanghai 201210, China, with the Shanghai Institute of Microsystem and Information Technology, Chinese Academy of Sciences, Shanghai 200050, China, and also with the University of Chinese Academy of Sciences, Beijing 100049, China (e-mail: xiezhy@shanghaitech.edu.cn).

Zhiqi Zhou, Linze Li, Zhuo Deng, and Baile Chen are with the School of Information Science and Technology, ShanghaiTech University, Shanghai 201210, China (e-mail: zhouzq@shanghaitech.edu.cn; lilz@shanghaitech.edu.cn; dengzhuo@shanghaitech.edu.cn; chenbl@shanghaitech.edu.cn).

Haiming Ji is with the University of Chinese Academy of Sciences, Beijing 100049, China (e-mail: jhm@semi.ac.cn).

Color versions of one or more figures in this article are available at <https://doi.org/10.1109/JSTQE.2021.3095470>.

Digital Object Identifier 10.1109/JSTQE.2021.3095470

Currently, p-i-n photodiodes (PDs) are commonly used as receivers (R_x) in the short-reach optical links. A Si p-i-n photodiode with a 3-dB bandwidth of ~ 19.1 GHz ($\text{FWHM}_{\text{Gaussian}} = 23$ ps) under a reverse bias of above 3 V and quantum efficiency of 52% at 850 nm wavelength has been demonstrated [4]. The device was integrated with periodic photon-trapping microstructures, which required a complicated fabrication process. Given the low absorption coefficient of Si at 850 nm (around 535 cm^{-1}), direct bandgap material GaAs is preferred to be used for 850 nm application. High-speed p-i-n photodiodes with GaAs/AlGaAs material system at 850 nm wavelength band have been demonstrated with the bandwidth of approximately 10 GHz to 30 GHz, depending on the device diameters [2]. The dark current of these devices is around 0.1 nA at -3 V, and the corresponding responsivity is 0.49 A/W, 0.52 A/W and 0.55 A/W for the devices with 1 μm , 1.6 μm and 2 μm intrinsic absorption layer, respectively. For high-speed operation, these p-i-n devices typically need a bias voltage of -2 V or -3 V to accelerate the carrier transport. In order to reduce power consumption and minimize system complexity of the receiver, zero-bias operation of the photodiodes is therefore desirable. Moreover, for the high-speed optical link used in the radiation environment, such as the High-Luminosity Large Hadron Collider (HL-LHC) project, low bias or zero-bias operation of optoelectronics devices are often needed to reduce the damage from radiation [5], [6].

Uni-traveling-carrier photodiodes (UTC-PDs) operating under low reverse bias voltage or zero bias operation have been demonstrated with high-speed and high-power performance at 1550 nm band, which is configured with a p-type photo-absorption layer and a wide bandgap electron collector layer [7]–[9]. In the 850 nm wavelength band, a 28 μm diameter GaAs/AlGaAs based UTC-PD has been demonstrated with a 3-dB bandwidth of 13 GHz and a responsivity of 0.32 A/W under zero-bias operation for 10 Gbit/s optical interconnect [10].

In this work, we demonstrate a zero-bias operational high-speed modified uni-traveling-carrier photodiode (MUTC-PD) based on GaAs/AlGaAs at 850 nm wavelength with a quantum efficiency of around 73%, which corresponds to a responsivity of 0.5 A/W. The 3-dB bandwidth is 22.5 GHz and 13.3 GHz for 20 μm and 40 μm diameter device, respectively. Compared with the other 850 nm zero biased devices with the same device diameter (28 μm) reported in reference [10], the 28 μm diameter device in this work shows a larger responsivity (0.5 A/W versus 0.32 A/W) and 3-dB bandwidth (17.9 GHz versus 13 GHz). The 40 μm diameter device, a typical size used in short-range communication, also exhibits a very low dark current of 75

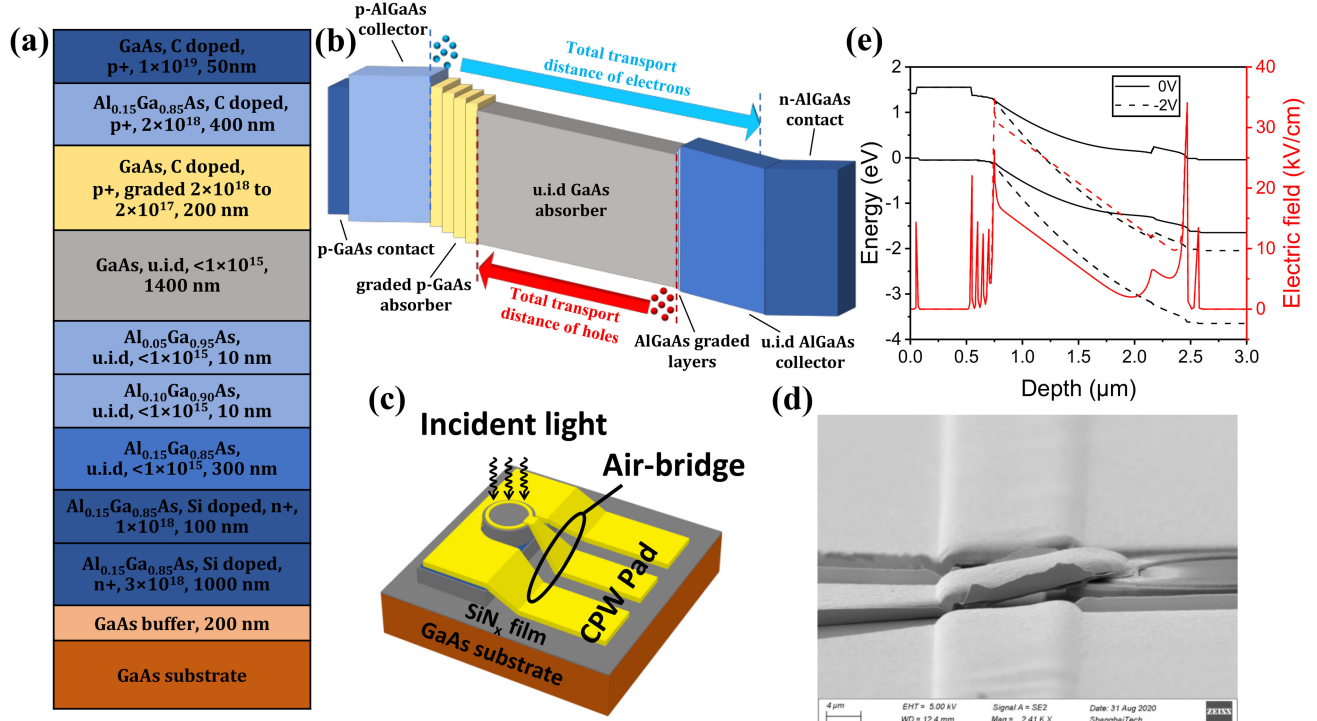


Fig. 1. Design for the device. (a) Epitaxial structure of the designed MUTC-PD. (b) Schematic band diagram of designed device. (c) Schematic diagram of the fabricated top-illuminated device. (d) SEM image of the fabricated device. (e) Stimulated energy band diagram and electric field of the device. Solid line: 0 V bias. Dash line: -2 V bias.

fA under -2 V bias. A clear eye pattern is demonstrated at a 25.8 Gbit/s data rate for the devices under zero-bias operation. The bandwidth limiting factors are also analyzed through the construction of an equivalent circuit model with the fitting parameters extracted from the S-parameter data.

II. DEVICE STRUCTURE

The epitaxial structure of the designed photodetector is shown in Fig. 1(a). The sample was grown on semi-insulating GaAs substrate by using metal-organic chemical vapor deposition (MOCVD) system. The epitaxial growth began with an 1100 nm thick n-type $\text{Al}_{0.15}\text{Ga}_{0.85}\text{As}$ bottom contact layer and a 300 nm un-intentionally doped $\text{Al}_{0.15}\text{Ga}_{0.85}\text{As}$ collection layer. Then, two 10 nm thick AlGaAs graded layers were grown followed by a $1.6 \mu\text{m}$ partially-depleted absorption layer, which consists of a $1.4 \mu\text{m}$ thick un-intentionally doped GaAs and four 50 nm p-type undepleted absorber layers with step grading doping profile of 2×10^{17} , 5×10^{17} , 1×10^{18} , and $2 \times 10^{18} \text{ cm}^{-3}$ to create a quasi-electric field that aids electron transport. After that, a 400 nm thick p-type $\text{Al}_{0.15}\text{Ga}_{0.85}\text{As}$ electron barrier was grown, and finally, the structure was capped by a 50 nm p-type GaAs top contact layer.

The schematic band diagram of the designed MUTC device is depicted in Fig. 1(b). Unlike the traditional p-i-n PDs, the photogenerated holes in the p-type GaAs could quickly respond within the dielectric relaxation time as the majority carriers. In this MUTC structure, $\text{Al}_{0.15}\text{Ga}_{0.85}\text{As}$ layer with a larger energy gap ($\sim 1.61\text{eV}$) was used as the collector layers, which is transparent to 850 nm wavelength light. On the other hand, the responsivity over 0.5 A/W of the device with a total $1.6 \mu\text{m}$

thickness GaAs absorber can be achieved with an anti-reflection coating. By properly choosing the thickness ratio of p-type GaAs and i-type GaAs, the transit time of holes can be designed to be roughly equal to that of electrons, thus improving the device bandwidth. The un-intentionally doped regions are expected to be fully depleted under zero bias with a concentration of around $1 \times 10^{15} \text{ cm}^{-3}$. Therefore, zero-bias operation of the designed MUTC-PD is expected with high responsivity and 3-dB bandwidth.

The sample was processed into a double mesa structure, with the schematic diagram and SEM picture shown in Fig. 1(c) and Fig. 1(d), respectively. The first mesa was stopped at the heavily n-doped $\text{Al}_{0.15}\text{Ga}_{0.85}\text{As}$ contact layer with induced coupled plasmas (ICP) dry etch process. The second mesa was terminated at the semi-insulating GaAs substrate through phosphoric acid-based wet etch ($\text{H}_3\text{PO}_4:\text{H}_2\text{O}_3:\text{H}_2\text{O} = 1:1:10$), which provides the isolation between devices. Ti/Pt/Au and GeAu/Ni/Au metal were deposited on top p+ doped GaAs and bottom n+ doped $\text{Al}_{0.15}\text{Ga}_{0.85}\text{As}$ contact layers, respectively, by using electron beam evaporation, which was followed by a rapid thermal annealing process to form a good ohmic contact. Sulfur passivation was used to reduce surface leakage current [11]. Then a 110 nm silicon nitride (SiN_x) film was deposited as an anti-reflection (AR) coating by plasma-enhanced chemical vapor deposition (PECVD). The devices were finally connected to a coplanar waveguide (CPW) pad of 50Ω characteristic impedance through an air-bridge structure.

Fig. 1(e) shows the simulated band diagrams for the device structure under 0 V and -2 V bias, where the concentration of un-intentionally doped regions was set to $1 \times 10^{15} \text{ cm}^{-3}$. It is shown that the un-intentionally doped $\text{Al}_{0.15}\text{Ga}_{0.85}\text{As}$ collector

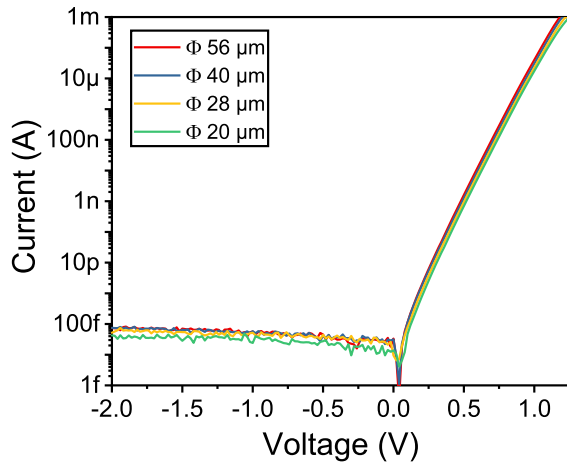


Fig. 2. Dark current versus voltage characteristic of the device with different diameters at room temperature.

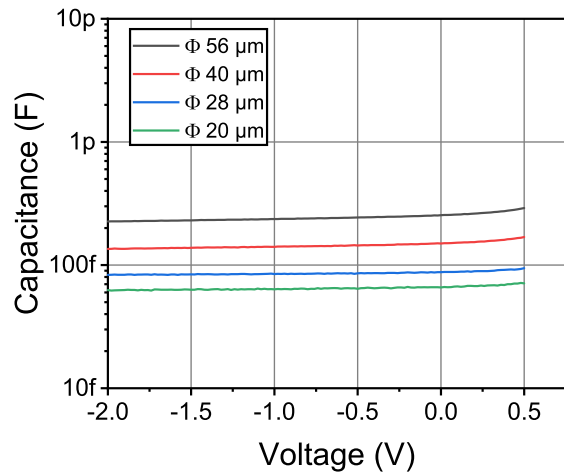


Fig. 3. Measured capacitance versus reverse bias for device with different diameters at room temperature.

layer and GaAs absorber can be fully depleted under zero-bias operation, which could meet the zero-bias operation mode of the designed MUTC-PD structure.

III. DEVICE CHARACTERIZATION

A. DC Electrical Characteristics

The dark current versus bias voltage characteristics at room temperature are shown in Fig. 2, which were measured in a probe station covered by an electromagnetic shield and recorded by a semiconductor device analyzer. The PDs show a low dark current at room temperature of 75 fA for the device with 40 μm diameter under -2 V bias, which is much lower than the previously reported p-i-n structure [2]. The corresponding dark current density is 6×10^{-9} A/cm².

Fig. 3 shows the capacitance-voltage curves measured at 1 MHz. The value of the capacitance remains almost constant as the reverse bias increases, which indicates the un-intentionally doped regions are fully depleted under zero bias.

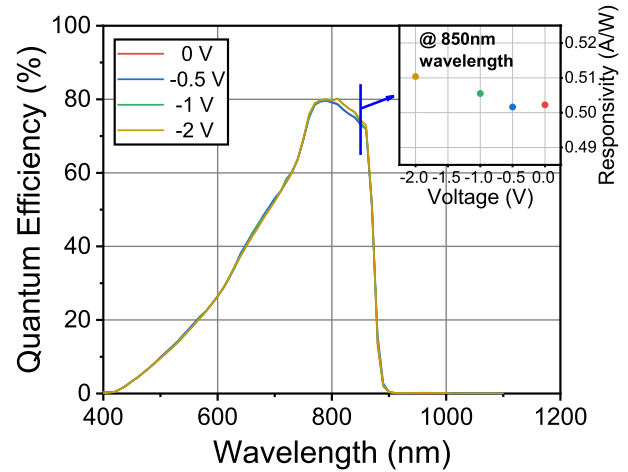


Fig. 4. Quantum efficiency of the device with 500 μm diameter at different bias voltage. The inset shows the responsivity versus bias voltage at 850 nm wavelength.

B. Quantum Efficiency

The quantum efficiency of the GaAs/AlGaAs MUTC-PD was measured by comparing the photoresponse of a 500 μm diameter device with that of a calibrated commercial Si photodiode. A tungsten lamp with a broadband spectrum followed by the grating spectrometer was used to generate a monochromatic light. The quantum efficiency of the device at the wavelength ranging from 400 nm to 1200 nm is shown in Fig. 4, where the typical quantum efficiency of the PDs at 850 nm is 73.2% under zero bias, corresponding to a responsivity of 0.502 A/W. The device exhibits a slight increase of responsivity up to 0.510 A/W as the reverse bias increases to -2 V. The absorption coefficient of GaAs absorber at 850 nm wavelength is estimated to be about 1×10^4 cm⁻¹, which is close to the previously reported value in reference [12].

C. Bandwidth

The frequency response of the device at room temperature was investigated by a calibrated system similar to references [13], [14]. A lensed fiber was used to couple the light to the device, where the optical source was generated by a DFB laser at 852 nm wavelength and modulated by an 850 nm Mach-Zehnder modulator (MZM). DC bias was supplied by a source meter through the external bias tee, while the RF signal was collected by the LCA system through an RF GSG probe. The values of the frequency-dependent loss of cables and GSG probe were carefully calibrated by a Vector Network Analyzer (VNA), while the loss of MZM, which was provided by the vendor, was subtracted from the measured data.

Fig. 5 shows the measured frequency response of the device with different diameters (20 to 56 μm) under 0 V and -2 V bias. The device with 40 μm and 20 μm diameter shows a 3-dB bandwidth of 13.3 GHz and 22.5 GHz under zero-bias operation, respectively. The 3-dB bandwidth of these devices increases to 19.1 GHz and 25.9 GHz under -2 V bias.

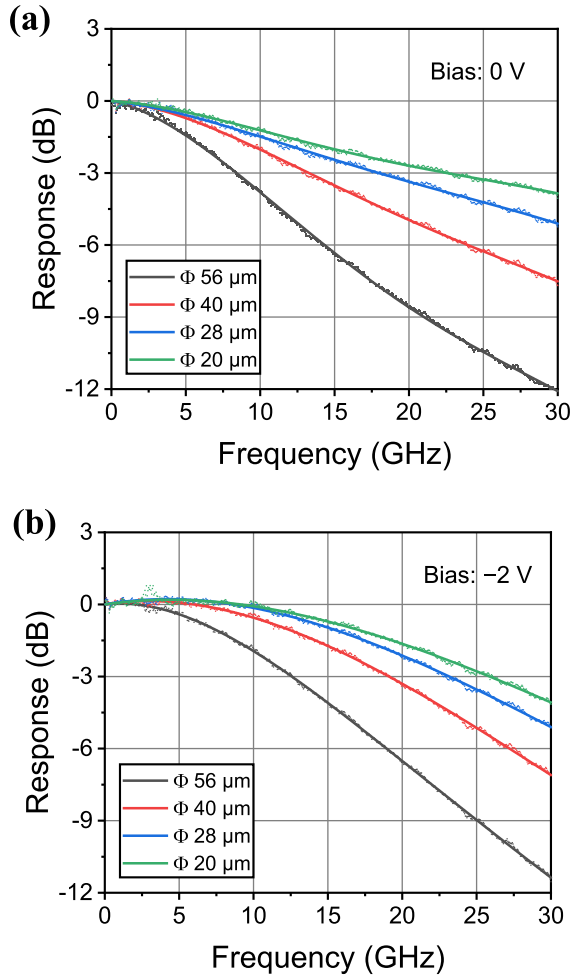


Fig. 5. Frequency responses of the device with different diameters under (a) zero bias and (b) -2 V bias.

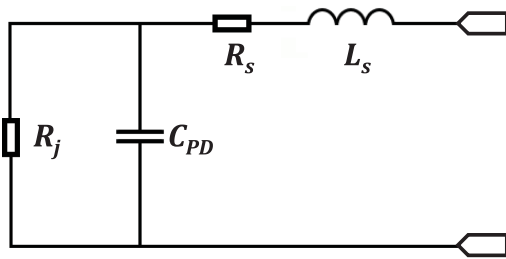


Fig. 6. Equivalent circuit model of the MUTC-PD for S11 fitting.

In order to study the bandwidth limiting factors of the MUTC-PDs, the scattering parameters (S11) of devices were measured by VNA. The parameter fitting was conducted in Advanced Design System (ADS) software with an equivalent circuit model as depicted in Fig. 6. The measured and fitted (smooth line) S11 data with 10 MHz-40 GHz frequency range of devices under zero bias are shown in Fig. 7. In the equivalent circuit model, R_s and L_s represent the series resistance and series inductance. C_{PD} is the total capacitance of the photodiode, including the parasitic capacitance and junction capacitance. The extracted

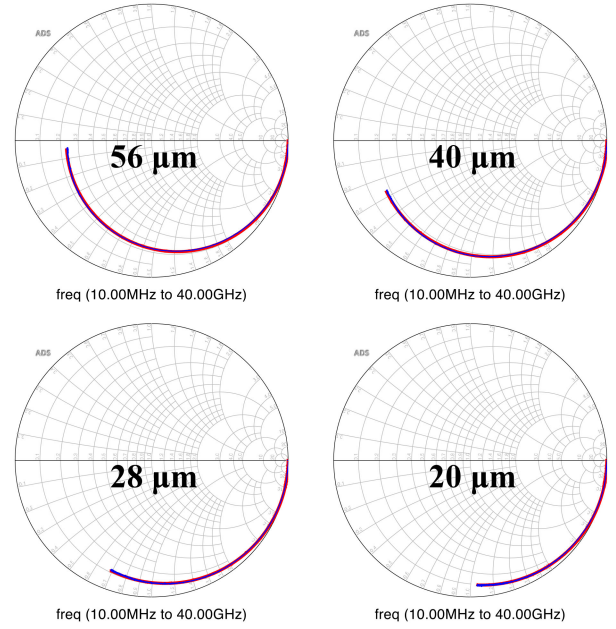


Fig. 7. Measured (blue line) and fitted (red line) S11 data with 10 MHz-40 GHz frequency range under zero bias voltage for the MUTC-PD with various diameter at room temperature.

TABLE I
FITTING PARAMETERS

Device Diameter (μm)	C_{PD} (fF)	R_s (Ω)	L_s (pH)
56	243.3	11.5	56.9
40	145.0	8.8	54.7
28	89.1	5.5	39.8
20	65.2	4.8	32.5

parameters are listed in Table I, where junction resistance (R_j) is typically very high (set to the order of 500 M Ω) given the low dark current of the device and is not listed in the table.

From the extracted capacitance in Table I and the measured capacitance of the device under zero bias (see Fig. 4), the parasitic capacitance (C_{st}) of 36.5 fF is determined from the intercept of the linear fit by plotting the total capacitances (C_{PD}) versus device areas, as shown in Fig. 8. This parasitic capacitance may originate from the air-bridge caused by a parasitic capacitor of the signal line and n-contact metal [15], which indicates further optimization of the fabrication processes may be necessary. The low values of R_s indicate good ohmic contact by the rapid thermal annealing process. The RC-limited frequency response is calculated using the equivalent circuit model with the extracted parameters, as shown in Fig. 9. The RC-limit-bandwidth of the 40 μm and 20 μm diameter device under zero bias are 20.9 GHz and 52.9 GHz, respectively.

Theoretically, the 3-dB bandwidth of the photodiode is limited by transit time and RC time, as expressed by the equation [16]:

$$\frac{1}{f_{3db}^2} = \frac{1}{f_{RC}^2} + \frac{1}{f_{tr}^2} \quad (1)$$

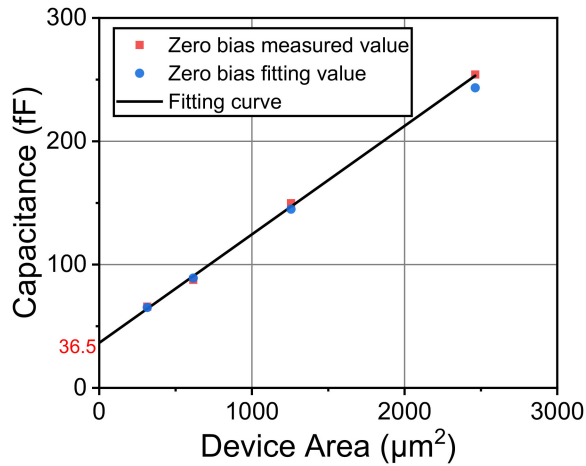


Fig. 8. Comparison of measured and fitting capacitances.

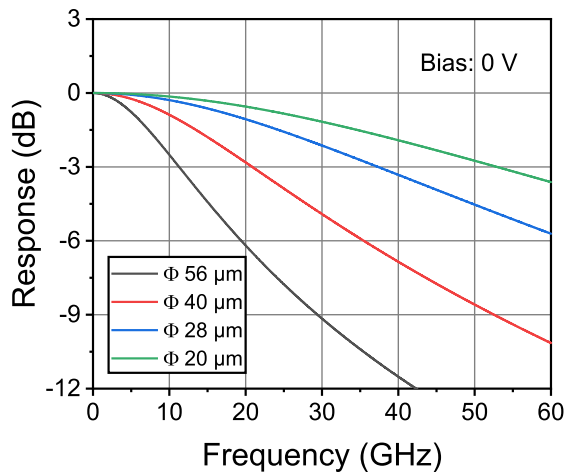


Fig. 9. Calculated RC limit frequency response with extracted circuit model parameters.

where f_{tr} , f_{RC} and f_{3dB} represent the transit-time-limited bandwidth, RC-limited bandwidth, and the total 3-dB bandwidth, respectively.

Fig. 10 shows the measured $1000/f_{3dB}^2$ versus the calculated $1000/f_{RC}^2$ values of the device. According to Equation (1), the transit-time-limited bandwidth can be determined as 24.1 GHz and 27.8 GHz under 0 V and -2 V bias, respectively, from the intercept of the linear fit of this figure. The various bandwidths (f_{3dB} , f_{tr} , f_{RC}) of devices versus diameter under different bias (from 0 V to -2 V) are plotted in Fig. 11. The slow increase of transit-time-limited bandwidth (f_{tr}) with bias can be attributed to the increase of transport velocity of the photogenerated carrier as bias increases. Meanwhile, the f_{tr} and f_{RC} of the 40 μm diameter device show similar values versus the bias, indicating that the 3-dB bandwidth of photodiodes with the diameter of 40 μm is limited both by the transit time and RC time, which meet the expectation of the designed epi-structure to balance of RC time and transit time for device with large size.

Fig. 12 shows the eye diagram of a 56 μm and 40 μm diameter device under zero bias operating at the data rate of 25.8 Gbit/s.

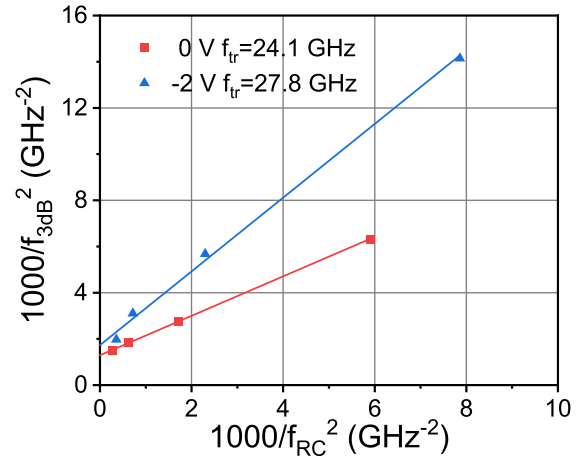
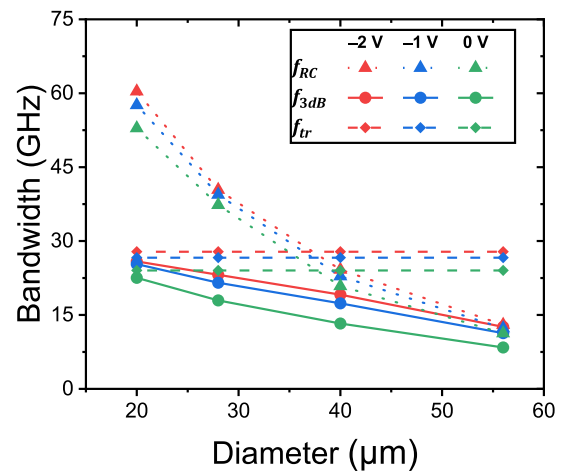
Fig. 10. The calculated ($1000/f_{RC}^2$) versus measured ($1000/f_{3dB}^2$) of devices under 0 V and -2 V bias voltage.

Fig. 11. RC-limited-bandwidth (dot lines), 3-dB bandwidth (solid lines) and transit-time-limited bandwidth (dash line) of devices versus device diameter.

The average photocurrent is about 390 μA . The optical signal was generated by a commercial 850 nm high-speed VCSEL module, connected with an OM3 multimode fiber (HGTECH 25G SFP28 AOC). The $2^{15}-1$ pseudo-random binary sequence (PRBS) patterns were generated by an arbitrary waveform generator (AWG) as the data source to drive the 850 nm VCSEL in the module. The output RF signal of the photodiode was amplified by a +23 dB microwave amplifier and then displayed on the real-time sampling oscilloscope. A clear eye pattern is demonstrated at a 25.8 Gbit/s data rate, which indicates the devices can be used in the 850 nm optical communications system under zero-bias operation.

The performance comparison of the MUTC device with other high-speed photodiodes at 850 nm wavelength under zero-bias operation with different structures or materials has been listed in Table II. Compared with the previously reported photodiodes, our device exhibits a much lower dark current and higher responsivity while maintaining a similar 3-dB bandwidth with a larger diameter (40 μm) under zero bias.

TABLE II
PERFORMANCE COMPARISON OF HIGH-SPEED PHOTODIODES AT 850NM WAVELENGTH

Ref.	Device parameter	Diameter (μm)	3dB-bandwidth (GHz)	Responsivity / Quantum efficiency @ 0 V	Dark current
[4]	Si p-i-n	30	~ 19.1 @ -3 V	52 %	0.06 nA @ -5 V
[17]	GaAs/InGaP p-i-n	15	9 @ 0 V	0.2 A/W	~ 1 nA @ -1 V
[18]	GaAs/AlGaAs UTC	28	9 @ 0 V	0.41 A/W	NA
[10, 19]	GaAs/AlGaAs UTC	28	13 @ 0 V	0.32 A/W	NA
This work	GaAs/AlGaAs MUTC	40	13.3 @ 0 V and 19.1 @ -2 V	0.50 A/W / 73.2 %	75 fA @ -2 V
		28	17.9 @ 0 V and 23.2 @ -2 V		52 fA @ -2 V

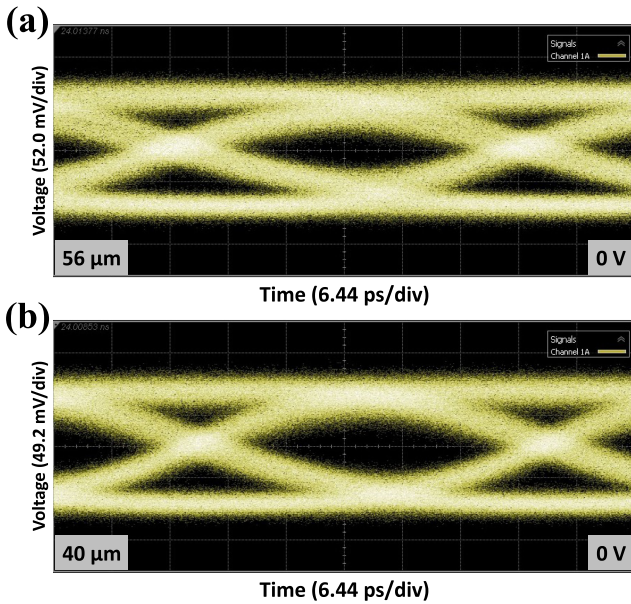


Fig. 12. Eye pattern at 25.8 Gbit/s data rate of the MUTC-PD under zero bias with the diameter of (a) $56 \mu\text{m}$ and (b) $40 \mu\text{m}$.

IV. CONCLUSION

In this work, we have demonstrated high-speed and low dark current MUTC-PDs based on GaAs/AlGaAs at 850 nm wavelength operating under zero-bias with a responsivity of ~ 0.5 A/W. The $20 \mu\text{m}$ and $40 \mu\text{m}$ diameter device exhibits a 3-dB bandwidth of 22.5 GHz and 13.3 GHz under zero-bias operation, respectively. Moreover, a clear eye pattern is demonstrated at a 25.8 Gbit/s data rate for $56 \mu\text{m}$ and $40 \mu\text{m}$ diameter device under zero-bias operation. Excellent performances of the devices suggest that these MUTC-PDs can be used in the 850 nm wavelength optical communications system with zero electrical power consumption.

REFERENCES

- [1] M. A. Taubenblatt, "Optical interconnects for high-performance computing," *J. Lightw. Technol.*, vol. 30, no. 4, pp. 448–457, Feb. 2012.
- [2] N. Dupuis *et al.*, "Exploring the limits of high-speed receivers for multimode VCSEL-based optical links," in *Proc. Opt. Fiber Commun. Conf.*, San Francisco, CA, USA: Optical Society of America, 2014, Paper M3G. 5.
- [3] M. Liu, C. Y. Wang, M. Feng, and N. Holonyak, "850 nm Oxide-Confined VCSELs with 50 Gb/s error-free transmission operating up to 85°C ," in *Proc. Conf. Lasers Electro-Opt.*, San Jose, CA: Optical Society of America, 2016, Paper SFIL.6.

- [4] Y. Gao *et al.*, "Photon-trapping microstructures enable high-speed high-efficiency silicon photodiodes," *Nature Photon.*, vol. 11, no. 5, pp. 301–308, 2017.
- [5] K. Gill *et al.*, "Radiation damage studies of optoelectronic components for the CMS tracker optical links," in *Proc. RADECS 97. 4th Eur. Conf. Radiat. its Effects Compon. Syst. (Cat. No. 97TH8294)*, 1997, IEEE, pp. 405–412.
- [6] F. Vasey *et al.*, "Development of radiation-hard optical links for the CMS tracker at CERN," *IEEE Trans. Nucl. Sci.*, vol. 45, no. 3, pp. 331–337, Jun. 1998.
- [7] T. Umezawa *et al.*, "Zero-bias operational ultra-broadband UTC-PD above 110 GHz for high symbol rate PD-array in high-density photonic integration," in *Proc. Opt. Fiber Commun. Conf. Exhib. (OFC)*, Los Angeles, CA, USA, 2015, IEEE, pp. 1–3.
- [8] J.-M. Wun, R.-L. Chao, Y.-W. Wang, Y.-H. Chen, and J.-W. Shi, "Type-II gaas. 0.5Sb0.5InP uni-traveling carrier photodiodes with sub-terahertz bandwidth and high-power performance under zero-bias operation," *J. Lightw. Technol.*, vol. 35, no. 4, pp. 711–716, Feb. 2016.
- [9] F. Yu, K. Sun, Q. Yu, and A. Beling, "High-speed evanescently-coupled waveguide Type-II MUTC photodiodes for zero-bias operation," *J. Lightw. Technol.*, vol. 38, no. 24, pp. 6827–6832, Dec. 2020.
- [10] F. Kuo, T. Hsu, and J. Shi, "A gaas/algaas based uni-traveling-carrier photodiode for 10Gbit/sec optical interconnect at 850nm wavelength with zero electrical power consumption," in *Proc. Opt. Fiber Commun. Conf.*, San Diego, CA, USA: Optical Society of America, 2009, Paper OWX5.
- [11] H. Oigawa, J.-F. Fan, Y. Nannichi, H. Sugahara, and M. Oshima, "Universal passivation effect of (NH₄)₂Sx treatment on the surface of III-V compound semiconductors," *Jpn. J. Appl. Phys.*, vol. 30, no. Part 2, no. 3A, pp. L322–L325, 1991.
- [12] H. C. Casey, D. D. Sell, and K. W. Wecht, "Concentration dependence of the absorption coefficient for n- and p-type GaAs between 1.3 and 1.6 eV," *J. Appl. Phys.*, vol. 46, no. 1, pp. 250–257, 1975.
- [13] Y. Chen *et al.*, "High-speed mid-infrared interband cascade photodetector based on inas/gaasb Type-II superlattice," *J. Lightw. Technol.*, vol. 38, no. 4, pp. 939–945, Feb. 2020.
- [14] Z. Xie *et al.*, "High-speed mid-wave infrared interband cascade photodetector at room temperature," *Opt. Exp.*, vol. 28, no. 24, pp. 36915–36923, 2020.
- [15] Y. Chen, Z. Xie, J. Huang, Z. Deng, and B. Chen, "High-speed uni-traveling carrier photodiode for $2 \mu\text{m}$ wavelength application," *Optica*, vol. 6, no. 7, pp. 884–889, 2019.
- [16] K. Kato, S. Hata, K. Kawano, and A. Kozen, "Design of ultrawide-band, high-sensitivity p-i-n photodetectors," *IEICE Trans. Electron.*, vol. E76-C, pp. 214–221, 1993.
- [17] J.-W. Shi, J.-M. Wun, C.-Y. Tsai, and J. E. Bowers, "GaAs/In_{0.5}Ga_{0.5}P laser power converter with undercut mesa for simultaneous high-speed data detection and DC electrical power generation," *IEEE Electron Device Lett.*, vol. 33, no. 4, pp. 561–563, Apr. 2012.
- [18] J.-W. Shi, F.-M. Kuo, C.-S. Yang, S.-S. Lo, and C.-L. Pan, "Dynamic analysis of cascaded laser power converters for simultaneous high-speed data detection and optical-to-electrical DC power generation," *IEEE Trans. Electron Devices*, vol. 58, no. 7, pp. 2049–2056, Jul. 2011.
- [19] J.-W. Shi *et al.*, "The monolithic integration of gaas-algaas-Based untraveling-carrier photodiodes with zn-diffusion vertical-cavity surface-emitting lasers with extremely high data rate/power consumption ratios," *IEEE Photon. Technol. Lett.*, vol. 21, no. 19, pp. 1444–1446, Oct. 2009.

Zhiyang Xie received the B.S. degree in optoelectronic engineering from the Huazhong University of Science and Technology, Wuhan, China, in 2017. He is currently working toward the Ph.D. degree with the School of Information Science and Technology, ShanghaiTech University, Shanghai, China. His research interest focused on high-speed photodiodes of III–V semiconductors.

Zhiqi Zhou received the B.S. degree from Jiangsu University in 2019. He is currently working toward the M.S. degree in Electronics Science and Technology with ShanghaiTech University. His research interests focus on uni-traveling carrier photodiode (UTC-PD).

Linze Li received the B.S. degree from ShanghaiTech University in 2020. He is currently working toward the M.S. degree in Electronics Science and Technology with ShanghaiTech University, and working mainly on uni-traveling carrier photodiode (UTC-PD).

Zhuo Deng received the B.Sc. and Ph.D. degrees from the The University of Hong Kong, Hong Kong, in 2010 and 2015, respectively. In 2015, he was a Research Associate with the Department of Physics, The University of Hong Kong, where he has been involved in multi-junction photovoltaic based on III-V compound semiconductors. In 2016, he joined the School of Information Science and Technology, ShanghaiTech University, Shanghai, China, as a Research Fellow. His current research interests include the optical properties of III-V compound semiconductors and the design, fabrication, and characterization of infrared photodetectors based on III-V compound semiconductor nanostructures.

Baile Chen received the bachelor's degree in physics from the Department of Modern Physics, University of Science and Technology of China, Hefei, China, in 2007, and the master's degree in physics and the Ph.D. degree in electrical engineering from the University of Virginia, Charlottesville, VA, USA, in 2009 and 2013, respectively. In February 2013, he joined Qorvo Inc., Bend, OR, USA, as an RF Product Development Engineer working on various RF power amplifiers and BAW filters for RF wireless communication systems. In January 2016, he joined the School of Information Science and Technology, ShanghaiTech University as a Tenure Track Assistant Professor, PI. His research interests include III-V compound semiconductor materials and devices, and silicon photonics.